Parametric instability of an elongated pool of liquid metal in a low frequency magnetic field

K. Spragg,Y. Fautrelle, A. Sneyd

EPM-SIMAP
ENSHMG - BP 75 - 38402 Saint-Martin d'Hères cedex, France
kirk.spragg@hmg.inpg.fr

Abstract :

Preliminary experimental work demonstrates the existence of parametric instabilities on the edge of a elongated pool of liquid metal which are driven by a low frequency vertical magnetic field. These instabilities cause the formation of varicose (V) and sinuous (S) modes on the edge of the pool.
We present a theoretical investigation of the parametric instabilities by considering a strip of liquid metal in the presence of a vertical, uniform, low frequency magnetic field. From our model we determine the threshold value of magnetic field strength required to excite various various modes.

Résumé :

Le travail expérimental préliminaire démontre l'existence d'instabilités paramétriques sur le bord d'une goutte ovale de métal liquide soumis à un champ magnétique vericale à frequence basse. Ces instabilités causent la formation des modes variqueux (V) et les modes sinueux (S) sur le bord de la goutte.
Nous présentons une investigation théorique des instabilités paramétriques dans une band de métal liquide soumise à un champ magnétique vertical de fréquence basse. A partir de notre modèle nous déterminons la valeur du seuil du champ magnétique necessaire pour exciter de modes divers.

Key-words :

Parametric instabilities; Free surface; Electromagnetic

1 Introduction

Preliminary experimental investigations of the parametric instabilities in an elongated mercury pool forced by a low frequency uniform alternating magnetic field, indicate the existence of two distinct azimuthal wave structures: Varicose (V) and sinuous (S) modes. Examples of both are given in figures 1(a) and 1(b). These observed instabilities are closely related to those observed by Fautrelle *et al.* (2005) in their experimental investigation of a circular pool of liquid mercury, which became known as the "starfish" problem. A theoretical investigation was performed by A.D. Sneyd & Fautrelle (2003), and we extend the Lagrangian method used to our geometry and superimpose infinitesimal azimuthal waves on the edges to model the growth of various V and S modes.

The parameter space consists of three quantities:

1. pool width w,
2. coil current or equivalently magnetic field strength (RMS) B_{eff},
3. the magnetic field frequency f or angular frequency $\omega = 2\pi f$,

where the predominate pool behaviour is determined by the parameters above. Experimental observations suggest the presence of two regimes:

(a) Mode 3S. (b) Mode 3V.

Figure 1: Sample of experimental observations.

(1) For weak magnetic fields amplitude or low frequency magnetic fields ($f \leq 2$) the free-surface pattern consists of forced oscillations of the average pool width x_0. The frequency of the forced oscillations is equal to the oscillation frequency of the electromagnetic forces (twice the frequency of the magnetic field).

(2) When the magnetic field reaches a given threshold, stationary non-symmetric surface waves appear along the edges of the pool (figure 1). We define the mode number n as the number of *half* cosine waves observed on one side of the pool. The wave shapes are regular, may be clearly identified, and can be classified into two types: V modes which are symmetric about the middle of the pool (figures 1(b)) and S modes, which are asymmetric about the middle of the pool (figures 1(a)). The wave frequency is equal to that of the magnetic field (half of the Lorentz forces), as observed in Galpin & Fautrelle (1992) and Galpin *et al.* (1992).

2 The mathematical model

As a first attempt to model the strip we consider a rectangular strip. Resting on a substrate at $z = 0$ and extending to infinity along both directions of the y axis, the strip is in the presence of an uniform vertical alternating magnetic field $\boldsymbol{B} = B\sin(\omega t)\widehat{\mathbf{z}}$; B, ω and $\widehat{\mathbf{z}}$ denoting respectively the typical magnetic field strength, its frequency and the vertical unit vector. We assume the field frequency ω is sufficiently low so that field penetration is complete.

We assume the average pool width x_0 is much larger than the pool height h and thus neglect the curvature of the edge, which we take to be vertical. Ignoring the forced standing waves observed in experiments for analytic simplicity, we consider only the first type of motion, thus we assume that the upper surface $z = h(t)$ remains plane. We now derive the differential equations which govern the V modes, after briefly summarise changes required to consider S modes.

2.1 V modes

The characteristic property of V modes is that the pool deformation is symmetric about the y axis, as shown in figures 1(b). Thus we consider an idealised geometry of a small sinusoidal displacement of the edge $c(y)$ as shown in figure 2(a). The equation of the edge is thus $c(y) = x_0(t) + \epsilon b(t)\cos(ky)$, where ϵ is a small parameter such that $\epsilon b(t) << x_0(t)$ and $b(t)$ is a function to be determined. We define $l = 2\pi/k$ to denote the wavelength of the edge in the model.

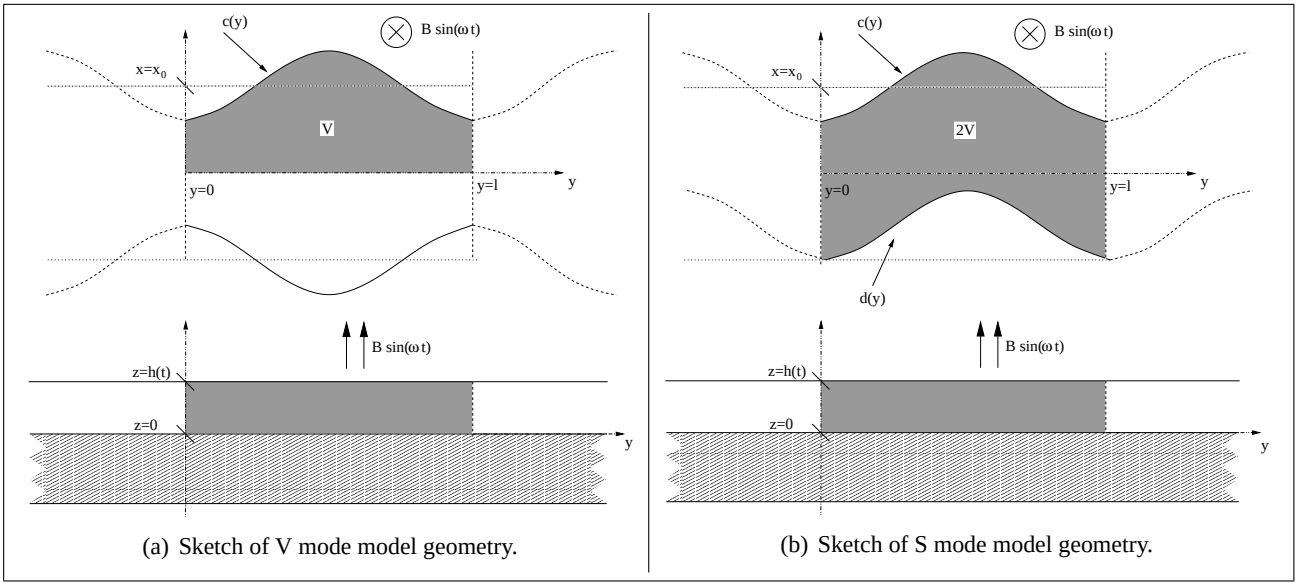

(a) Sketch of V mode model geometry.

(b) Sketch of S mode model geometry.

Figure 2: Simplifi ed geometries used in model S and V modes.

It follows from symmetry that the volume $V = hx_0l$. We assume that the fluid motion is inviscid and irrotational. We consider symmetric (about the y axis) oscillations in $h(t)$ and $x(t)$ - the strip broadening and becoming thinner or narrowing and becoming higher while conserving volume, and azimuthal oscillations in $b(t)$ induced by the oscillating magnetic field. We now define a Lagrangian function involving the kinetic, surface, gravitational and magnetic potential energies of the strip.

2.2 Gravitational and surface tension potential energy

Neglecting the edge contribution to surface tension, the surface tension and gravitational potential energy are simply: $E_\gamma + E_{grav} = V\left(2\gamma/h + \rho g h/2\right)$.

Minimising with respect to h gives an estimate of the rest height $h_0 = 2\sqrt{\gamma/\rho g}$ which is a reasonable approximation if $x_0 >> h$, which is the case in the experiments. However, to compute the contribution of the edge perturbation on E_γ we must integrate $h\gamma x$ along the edge $x = c(y)$. Doing so gives the following expression for the potential energy of the system:

$$E = \frac{1}{2}(1/h' + h') + \frac{1}{4}h'(l' + \frac{\pi}{2}\epsilon^2 k' b'^2), \tag{1}$$

where we have changed variables to the non-dimensional height $h' = h/h_0$ and time $t' = t/\sqrt{h_0/g}$, and $k' = h_0 k$, $l' = l/h_0$ and $b' = b/h_0$.

Velocity potential

Owing to the hypotheses used, the velocity field is governed by a harmonic scalar potential ϕ, which must satisfy the conditions:

$$\nabla^2\phi = 0, \qquad \left(\frac{\partial\phi}{\partial z}\right)_{z=h} = \dot{h}, \qquad \left(\frac{\partial\phi}{\partial z}\right)_{z=0} = 0, \qquad \left(\frac{\partial\phi}{\partial n}\right)_{x=c(y)} = v_n.$$

h The co-ordinate n is normal to the edge $x = c(y)$ and v_n is the velocity of a point on the edge. Expanding the velocity potential in the form, $\phi = \phi_0 + \epsilon\phi_1 + \ldots + \epsilon^m\phi_m \ldots$, and after much

algebra we obtain:

$$\phi_0 = \frac{\dot{h}}{2h}(z^2 - x^2), \qquad \phi_1 = C_1 \cos(ky)\cosh(kx), \text{ and } \phi_2 = C_2 \cos(2ky)\cosh(2kx) \quad (2)$$

to the second order in ϵ, where C_1 and C_2 are coefficients in b, h, x_0 and k. These are omitted for brevity.

2.3 Kinetic energy

We now proceed to calculate the kinetic energy of a wavelength section given by: $T = \frac{1}{2}\rho \int_S \phi \nabla\phi \cdot \mathrm{d}\mathbf{S}$. The lower surface $z = 0$ gives no contribution; by periodicity and symmetry, neither do the boundaries between sections. Thus we need only consider the surface integrals on the upper surface $z = h$ and of the edge along $c(y)$.

After some algebra and non-dimensionalising as before, we find that we can write the total kinetic energy as a quadratic form in $\dot{h}'$ and $\dot{b}'$,

$$T = Q_0 \dot{h}'^2 + \epsilon^2 \left(Q_1 \dot{h}'^2 + 2R\dot{h}'\dot{b}' + S\dot{b}'^2 \right), \quad (3)$$

where the non-dimensional coefficients Q_0, Q_1, R and S are non-dimensional coefficients in V, x_0, k, b and h and are omitted for brevity.

2.4 Electromagnetic potential energy

According to Fautrelle & Sneyd (2005), the electromagnetic body force $\mathbf{F}$ is given in the low frequency limit by $\mathbf{F} = \frac{1}{2}\rho\omega^2 \mathcal{N} \sin(2\omega t)\nabla\tau$, where $\mathcal{N} = \frac{\sigma B^2}{\rho\omega}$ is the non–dimensional interaction parameter, and $\tau(x, y)$ is the torsion function, which must satisfy, $\nabla^2\tau = -1$, $\tau(0, y) = 0$, and $\tau\big(c(y), y\big) =$ constant. It follows from that the potential energy U is given by $U = -\frac{1}{2}h\rho\omega^2\mathcal{N}\sin(2\omega t)\int_0^l \mathrm{d}y \int_0^{x_0+\epsilon b\cos(ky)} \tau \mathrm{d}x$. Upon taking a Taylor expansion of the boundary condition in ϵ, similarly expanding τ and solving $\nabla^2\tau = -1$ to the second order in ϵ we find

$$U = \frac{1}{12} V' \omega'^2 \mathcal{N} \sin(2\omega t) \left[x_0'^2 - 3\epsilon^2 b'^2 \left(1 - k' x_0' \tanh(k' x_0')\right) \right], \quad (4)$$

where we have non–dimensionalised as before and $\omega = \omega\sqrt{h_0/g}$, $x_0' = x_0/h_0$ and $V' = V/h_0^3$.

2.5 Lagrange equations

Using non–dimensional energies 1, 3 and 4, we now define a Lagrangian function $L(b, \dot{b}', h', \dot{h}')$ of our model as:

$$L = Q_0 \dot{h}'^2 + \epsilon^2 (Q_1 \dot{h}'^2 + 2R\dot{h}'\dot{b}' + S\dot{b}'^2) - E - U. \quad (5)$$

The resulting Euler-Lagrange equations are:

$$\frac{\partial}{\partial t'}\frac{\partial L}{\partial \dot{h}'} - \frac{\partial L}{\partial h'} = 0, \text{ and } \frac{\partial}{\partial t'}\frac{\partial L}{\partial \dot{b}'} - \frac{\partial L}{\partial b'} = 0. \quad (6)$$

These yield a coupled system consisting of two ODEs governing the forced symmetric oscillations of $h(t)$ and the asymmetric oscillations of the edge perturbation amplitude $b(t)$. Both are governed by the effects of surface tension and the magnetic field.

2.6 S modes

The geometry of a S mode is similar to that of a V mode in that the boundary at $x = x_0$ is perturbed to $x = c(y)$, but the boundary at $x = -x_0$ is perturbed to $x = d(y) = -x_0(t) + \epsilon b(t)\cos(ky)$, breaking the symmetry across the x axis as shown in figure 2(b). So in recalculating the various energies of the system one we must now consider the volume enclosed between both boundaries, i.e $2V$. The derivation of this model progresses in an otherwise identical manner to that of the S mode case.

2.7 Special cases

Two obvious special cases of the governing equations 5 exist: (1) where the edge perturbation is zero and (2) where pool depth h is taken to be constant and equal to h_0. For a small perturbation η from h_0 (1) reduces to simple harmonic oscillator: $\ddot{\eta} + \Omega'^2\eta = \frac{\mathcal{N}\omega'^2V'^2}{2(l'^2+V'^2)}\sin(2\omega' t')$ which is forced at twice the field frequency ans has natural frequency: $\Omega'^2 = l'^2\left(l'^2 + V'^2\right)^{-1}$. This estimates the natural frequency of the forced symmetric oscillations.

Case (2) reduces to a Mathieu equation in b of the form:

$$\ddot{b}' + b'\Omega'^2[1 - C\sin(2\omega' t')] = 0. \tag{7}$$

Where the dimensionless eigen frequency Ω' is given by: $\Omega'^2 = \Omega_V'^2 = \frac{\pi}{2V}k'^2x_0'\tanh(k'x_0')$ in the V-mode case and $\Omega'^2 = \Omega_S'^2 = \frac{\pi}{2V}k'^2x_0'\coth(k'x_0')$ in the S-mode case.

3 Results

Owing to their preliminary nature we are unable to present the results of the experiment work conducted, but can present some basic predictions from the model presented. We determine the stability threshold of various R and S modes using a Runge-Kutta 4 method to solve the ODEs 6 in order obtain a numerical solution for a given magnetic interaction parameter $\mathcal{N}$. For a fixed magnetic interaction parameter $\mathcal{N}$, if over a given time period say T, an initial perturbation, say b_0 of b reaches an amplitude 10 times its starting value, the solution is considered unstable (larger values up to 1000 were tried but did not significantly change the results). This method is used in conjunction with a bisection method to determine the stability of a given mode n at particular field frequency f.

In the absence of accurate experimental data we estimate the wavelength l_e of the edge wave corresponding to mode n by

$$l_e \approx \frac{L}{n}. \tag{8}$$

We use this estimate to obtain the theoretical stability diagram given in figure 3, where we have used pool parameters: length $L = 84mm$, width $w = 34mm$ and rest height $h_0 = 6.4mm$. We use the physical properties of the Gallium and Indium alloy used in the experiments. Is is composed of 12.5 % Indium and has the following physical properties: melting point $18°$C, density ρ 6054 $\mathrm{kg}\cdot\mathrm{m}^{-3}$, electrical conductivity σ $3.84\cdot10^6\Omega^{-1}\cdot\mathrm{m}^{-1}$, surface tension γ $0.6\mathrm{kg}\cdot\mathrm{m}^{-2}$ and viscosity ν $3.22\cdot10^{-7}\,\mathrm{m}^2\cdot\mathrm{s}^{-1}$. We use a time-step size of $5\cdot10^{-3}$s, a time period T of 400s, an initial perturbation $b_0 = 10^{-4}$ of b and $\epsilon = 0.01$. The stability diagram corresponds poorly with experiments, agreement would be improved if experimentally measured wavelengths were used in place of the estimate 8. These however are not yet available, however the natural frequency of the forced oscillations corresponded closely to that predicted.

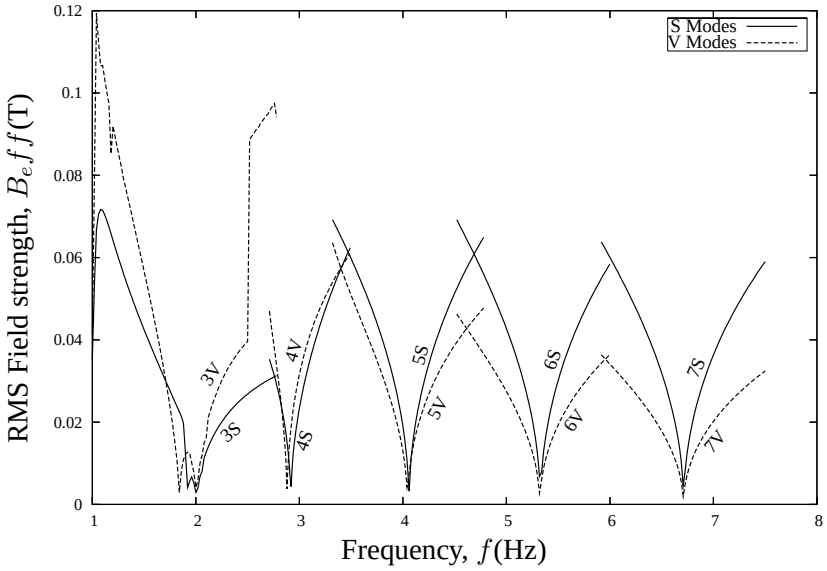

Figure 3: Numerical results using theoretical wavelengths.

4 Conclusion

The preliminary experimental investigations of the parametric instabilities of the free surface of liquid metal strip has revealed two main azimuthal wave structures: varicose (V) and sinuous (S) wave modes. In a simplified geometry, we derive a mathematical model of this phenomena and present a stability diagram for various modes of both types using a linear stability analysis. The results compare only qualitatively to those of the experiments, the estimation of the eigen-frequency of the forced modes is close to that observed but the stability diagram corresponds poorly. Our simple estimation of wavelength ignores end effects and is certainly a poor estimation. Thus we expect that using experimentally measured wavelengths with our model will produce a stability diagram which has mode transitions in a similar order as those observed.

References

A.D. SNEYD, J. E. & FAUTRELLE, Y. 2003 The starfish experiment: a Lagrangian approach. *Magnitnaya Girodynamika* **39** (3), 271–278.

FAUTRELLE, Y., ETAY, J. & DAUGAN, S. 2005 Free-surface horizontal waves generated by low-frequency alternating magnetic fields. *J. Fluid Mech.* **527**, 285–301.

FAUTRELLE, Y. & SNEYD, A. 2005 Surface waves created by low-frequency magnetic fields. *European Journal of Mechanics B - Fluids.* **24**, 91–112.

GALPIN, J. & FAUTRELLE, Y. 1992 Liquid-metal flows induced by low-frequency alternating magnetic fields. *J. Fluid Mech.* **239**, 383–408.

GALPIN, J., FAUTRELLE, Y. & SNEYD, A. 1992 Parametric resonance in low-frequency magnetic stirring. *J. Fluid Mech.* **239**, 409–427.